NANO LETTERS

Letter

pubs.acs.org/NanoLett

Dynamically Tracking the Strain Across the Metal–Insulator Transition in VO_2 Measured Using Electromechanical Resonators

Pritesh Parikh,[†,‡,∥] Chitraleema Chakraborty,[†,∥] T. S. Abhilash,[†] Shamashis Sengupta,*[,†] Chun Cheng,[§] Junqiao Wu,[§] and Mandar M. Deshmukh*[,†]

[†]Department of Condensed Matter Physics and Materials Science, Tata Institute of Fundamental Research, Mumbai 400005, India

[‡]Birla Institute of Technology and Science - Pilani, Hyderabad 500078, India

[§]Department of Materials Science and Engineering, University of California, Berkeley, California 94720, United States

Supporting Information

ABSTRACT: We study the strain state of doubly clamped VO_2 nanobeam devices by dynamically probing resonant frequency of the nanoscale electromechanical device across the metal–insulator transition. Simultaneous resistance and resonance measurements indicate M1–M2 phase transition in the insulating state with a drop in resonant frequency concomitant with an increase in resistance. The resonant frequency increases by ~7 MHz with the growth of metallic domain (M2–R transition) due to the development of tensile strain in the nanobeam. Our approach to dynamically track strain coupled with simultaneous resistance and resonance measurements using electromechanical resonators enables the study of lattice-involved interactions more precisely than static strain measurements. This technique can be extended to other phase change systems important for device applications.

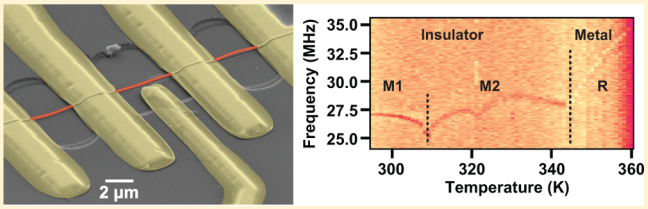

KEYWORDS: *VO_2, NEMS, lattice softening, phase transition, metal–insulator transition*

The metal–insulator transition in vanadium dioxide (VO_2) is characterized by a change in the crystal structure and a variation in the conductivity by several orders of magnitude. A strain-free VO_2 crystal undergoes a transition from the low-temperature insulating monoclinic phase to the high-temperature metallic rutile phase close to 341 K. Across the phase transition from insulator to metal, the length of the crystal shrinks by 1% along the *c*-axis of the high-temperature phase (rutile).[1−4] The conductance properties of VO_2 are strongly dependent upon the elastic strain, which greatly affects the phase transition temperature as well.[5] Experiments have demonstrated the percolative nature of the transition where metal and insulator domains coexist at temperatures near the transition.[6−8] In recent years, the realization of VO_2 single crystalline nanobeams have caused an interesting development in this research area. These show individual metal and insulator domains existing along the length of the nanowire, which have been imaged.[9] Recent experimental studies have demonstrated electric field-induced transition in VO_2 nanobeams as well as suppression of metal–insulator transition using electrolyte gating.[10−15] The nanowires can be strain engineered to tune the transition temperature.[16,17] This has opened up new avenues for device applications of VO_2.[18,19] The physics behind the insulating properties of VO_2 remains a widely debated topic with signatures of both Mott and Peierls mechanisms being detected in experiments.[20−24] Research on VO_2 nanobeams has revealed a rich phase diagram, highlighting the fact that the insulating phase can exist in two of the three different crystal structures, depending on the temperature and strain state of the lattice.[25] These phases can be expected to have different elastic and conduction properties.

In our work, we have studied nanoelectromechanical (NEM) resonators fabricated from VO_2 nanobeams. The aim is to track the temperature evolution of the resonant frequency in the insulating phase and across the development of a metal domain, which would yield information about the elastic response of the system while simultaneously measuring the resistance.

The VO_2 nanobeams used in our experiments are grown by the vapor-deposition technique and are initially embedded in a Si/SiO_2 substrate.[26] Electrodes are fabricated by electron beam lithography and buffered HF solution is used to etch the substrate underneath the nanobeams to suspend them. As the temperature is increased across the phase transition, the crystal shrinks in length, and in the metallic state the system is under tensile strain. Because of the finite strain in the nanobeam, the phase transition characteristics are different from a free crystal. Near T_{c0} (the transition temperature of an unstrained free crystal), instead of the entire system becoming metallic, only a metal domain appears. The domain grows in size until the entire nanobeam becomes metallic. The transition from the completely insulating to the completely metallic phase is accompanied by a change in the strain of 1%.

Received: June 11, 2013
Revised: August 30, 2013
Published: September 3, 2013

Over the past decade, NEMS devices have emerged as an active area of research with wide-ranging applications, like ultrasensitive mass detection,[27−29] realizing logic gates,[30] and studying the quantum ground state of a harmonic oscillator.[31] We use the frequency modulated (FM) mixing technique to actuate and detect mechanical motion.[32] For actuation, a side gate electrode is used. A frequency-modulated voltage V_{sd}^{FM} at frequency f, deviation f_Δ, and modulation rate f_r is applied at the source. $V_{sd}^{FM}(t) = V_0 \cos(2\pi f t + (f_\Delta/f_r)\sin(2\pi f_r t))$, where t denotes time and V_0 denotes the amplitude of the FM signal. A dc voltage V_g^{dc} is applied to the gate electrode, producing the driving force on the nanobeam (at frequency f). Because of heterodyne mixing, there is a low-frequency component of current (at frequency f_r), called the mixing current I_{mix}, through the device. ($f_r \sim$ few hundred hertz in our experiment.) I_{mix} demonstrates an abrupt change when the driving frequency f of V_{sd}^{FM} is close to the natural resonant frequency of the nanobeam[32]

$$I_{mix} \propto \frac{dG}{dq} f \frac{\left(f^2 - f_0^2 + \frac{f_0^2}{Q}\right)\left(f^2 - f_0^2 - \frac{f_0^2}{Q}\right)}{\left((f_0^2 - f^2)^2 + \left(\frac{ff_0}{Q}\right)^2\right)^2} \quad (1)$$

where G is the conductance, q is the capacitively induced charge, f_0 is the natural resonant frequency of the beam, and Q is the resonance quality factor. The amplitude of mechanical oscillation is maximum at f_0. This reflects on the mixing current as a sharp change. f_0 is related to the longitudinal elastic modulus E and strain η by the following relation

$$f_0 = \sqrt{\frac{EI}{\rho S}}\left(\frac{1}{2L}\sqrt{\eta\frac{S}{I}} + \frac{1}{L^2}\right) \quad (2)$$

where L is the length of the suspended nanobeam, I is the moment of inertia, S is the cross-sectional area, and ρ is the mass density.[33]

The circuit used for simultaneous measurement of resistance and resonance is shown in Figure 1a. The dc voltage V_0 drives a current through the device (in series with a large resistance R), and the voltage drop is measured across the nanobeam to determine its resistance. Figure 1b shows the temperature-dependent resistance of the device measured in the four probe geometry and inset shows the scanning electron microscope image of a resonator fabricated with a local side gate. As seen from the plot, the device undergoes a metal−insulator transition. Abrupt changes in resistance occur at 353 K and 338 K during the heating and cooling cycle respectively. An increase in resistance is also observed in the insulating phase. Because of a pronounced buckling in the nanobeam (refer to Supporting Information Section 1 for SEM images), Figure 1b closely resembles the dynamics of a strain-free crystal that has a sharp transition without the formation of metallic domains (refer to Supporting Information Section 5 for more devices showing the abrupt transition from insulating to metallic state). The beam buckling mechanics itself is already complicated; strain is nonuniform in both thickness and length direction of the VO_2 nanobeam, therefore it is very difficult to quantitatively describe the M1−M2 process in the buckled beam. But in general, when increasing temperature, a M1−M2 mixed system should grow in M2 percentage, as seen from the fact that the M1/M2 phase boundary has a negative slope with respect to temperature. However, whether this is manifested as a weakly

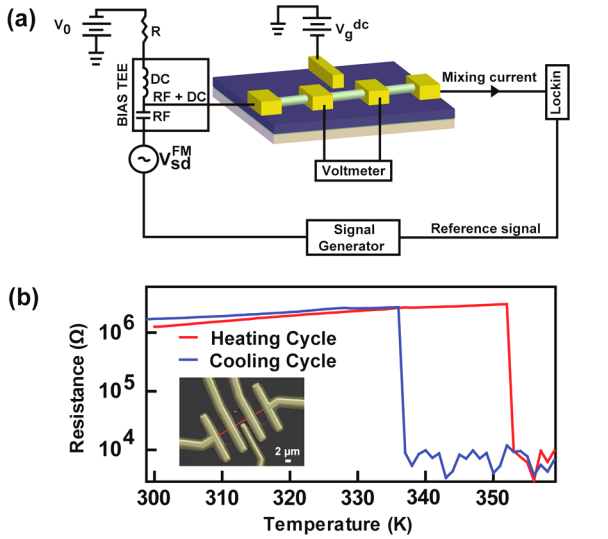

Figure 1. (a) Schematic of the circuit used for simultaneous resistance and resonance measurements. (b) Temperature versus resistance plot across the metal−insulator transition and inset shows SEM image of a side gated VO_2 nanobeam resonator. Pronounced buckling observed in the nanobeam (refer to Supporting Information Section 1 for more details) causes it to closely resemble the dynamics of a strain-free crystal that has a sharp transition without the formation of metallic domains. The increase in resistance below 355 K can be attributed to nonuniformity in the strain in both thickness and length of the VO_2 nanobeam.

metallic behavior depends on the details of domain structure and initial bending configuration. Some other device would show such metallic behavior only within a narrow temperature window. There is also an observable hysteresis in the variation of resistance with temperature.[15,34]

In Figure 2, we plot the resonance characteristics of a nanobeam device. The nanobeam is initially in a strained state (absence of buckling) (refer to Supporting Information Section 1 for more details). To measure the change in strain of the nanobeam across the metal−insulator transition, I_{mix} is measured as a function of the driving frequency f and the resonant frequency is tracked by varying the temperature (Figure 2a,b). The large increase in frequency beyond 343 K is a consequence of the increase in the strain of the nanobeam. A metal domain appears in this temperature range and the nanobeam shrinks along its length. As the size of the metal domain grows with increase in temperature, the intrinsic length of the nanobeam starts reducing and the strain is enhanced. This shows up as a sudden increase in the resonant frequency (Figure 2a,b). It has been reported that the elastic modulus of both the insulator and metal phases are similar,[35,36] and hence, the change in resonant frequency is assumed here to be primarily due to the change in strain.

The conductance was checked along with the resonant frequency, by measuring the mixing current as a function of driving frequency (for resonance data) simultaneously with the resistance of the device. The resistance is measured using the two probe geometry (Figure 2c). The presence of strain causes the metal−insulator transition to proceed via the formation of metallic domains leading to a gradual change in the resistance.[16] Noticeable features were seen in both resistance and resonant frequency at similar temperatures (Figure 2). Figure 2d shows the phase diagram for VO_2 with temperature as a function of stress and strain.[6] The blue line indicates a possible trajectory of

dx.doi.org/10.1021/nl402116f | Nano Lett. 2013, 13, 4685−4689

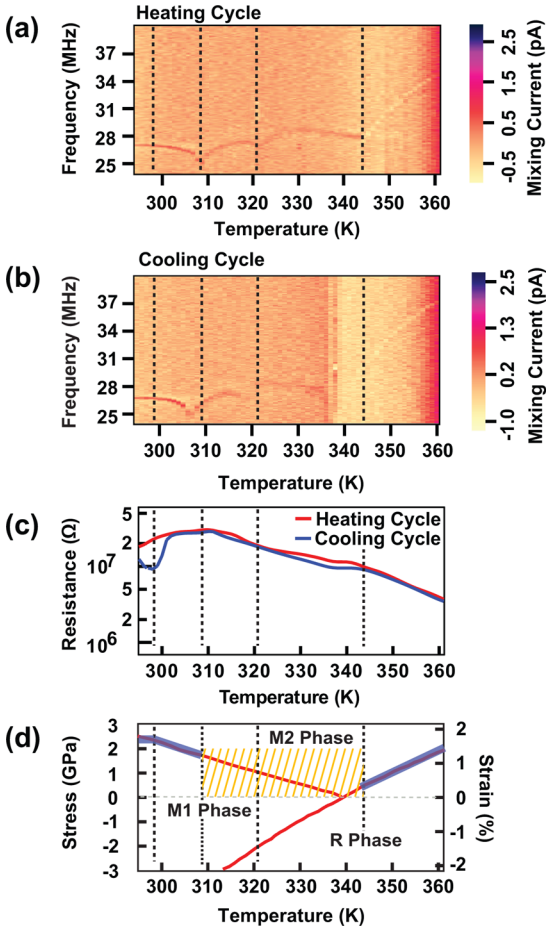

Figure 2. Device 1: (a) The change in resonant frequency with temperature during heating cycle. (b) Measured resonance response across the metal−insulator transition during cooling cycle. The sharp change beyond 343 K results from the change in strain due to the appearance of a metal domain. (The plots shown here for resonant frequency are background subtracted for clarity.) (c) The change in resistance is measured in two probe geometry simultaneously with the resonance response. (d) Depicts the phase diagram of VO_2 with temperature as a function of stress and strain (following ref 6). The red line indicates the phase separation boundaries. The blue line indicates the proposed trajectory of our device. As indicated by the orange region, we do not have a comprehensive microscopic understanding of the features between 310 K and 340 K.

our device across the phase diagram. The increase in frequency above 343 K (in Figure 2a) indicates a coexistence of metal and insulator domains, corresponding to an evolution of the system along the M2−R phase boundary.

There are interesting features in the insulating state also. We see a clear dip in f_0 at 309 K (Figure 2a). The temperature range at which the dip is seen in well inside the insulating phase. Atkin at el.[5] had shown by micro-Raman spectroscopy studies that the insulating state of VO_2 may be in one of two possible monoclinic phases (M1 and M2). Below 305 K, a third triclinic T phase is also possible. The state of the system is determined by the two parameters of temperature and strain. In order to understand the changes in the resonant frequency in the insulating phase, we refer to the phase diagram[6] of VO_2 (Figure 2d). From 295 K to 309 K, the resistance of the nanobeam increases with a concurrent decrease in the resonant frequency. This suggests a transition from the M1 to the M2 phase. The increase in resistance is a result of a higher resistance for the M2 phase as compared to the M1 phase.[6] Moreover the transition from M1 to M2 phase causes an increase in the length of the nanobeam reducing the strain by 0.3%.[37] This reduction in strain is reflected by a dip in the resonant frequency at 309 K. At this temperature, the VO_2 nanobeam sees a growth of the M2 insulating phase.

We do not have a complete microscopic understanding of the rich features between 310 K and 340 K (the region represented by orange in Figure 2d). A possible explanation for the dip in resonant frequency at 320 K could be due to the phonon softening predicted for strongly correlated electron systems.[38,39] At 343 K, the transition from M2 to R phase starts with the appearance of a metal domain, resulting in a rapid increase of the strain in the nanobeam. This is also reflected by a kink in the resistance at 343 K (Figure 2c). The propagation of the domain wall through the length of the nanobeam may have an important role to play in determining the temperature variation of the resonant frequency (Guo et al.[25] had reported superelasticity at an M1−M2 domain wall). It is possible that in an analogous way, the dip at the metal−insulator transition may also be related to the elastic behavior of the domain wall. The development of an M2 phase at 309 K requires a large strain of 1% (from the phase diagram, ref 6), whereas the resonant frequency values suggest a smaller strain of 0.2%. The reason for this difference is not understood at present and further studies are required to understand in detail the properties of the insulating phase.

To model the mechanical response of the system accompanying the growth of the metal domain, we need to understand how the strain changes with temperature. We denote by x the fraction of the length of the nanobeam that has become metallic. With a prestrain of ε_i in the insulating state, the total strain at a temperature T is given by $\varepsilon_T = \varepsilon_i + \varepsilon_0 x$ (ε_0 = 1%, the fractional change in length between the insulator and metal states.) In the following calculation, g_I and g_M represent the free energy densities (energy per unit volume) of the insulator and metal phases respectively. L, w, and t are the length, width, and thickness of the beam. The total energy of the system is

$$\Sigma = g_I Lwt(1 - x) + g_M Lwtx + \frac{1}{2}E(\varepsilon_i + \varepsilon_0 x)^2 Lwt + \Sigma_{wall} \quad (3)$$

where Σ_{wall} is the energy of a domain wall boundary. The latent heat of phase transition H is given by

$$H = (g_I - g_M)\frac{T_{c0}}{T - T_{c0}} \quad (4)$$

Minimization of energy from eq 3 and using eq 4 yields the following result for the fractional length of the metal domain

$$x = \frac{H}{E\varepsilon_0^2 T_{c0}}(T - T_{c1}) \quad (5)$$

with T_{c1} being given by

$$T_{c1} = \frac{\varepsilon_i \varepsilon_0 E T_{c0}}{H} + T_{c0} \quad (6)$$

T_{c1} is the temperature at which the metal domain starts to grow. $T_{c1} < T_{c0}$ (or $T_{c1} > T_{c0}$) when the initial strain is compressive (or tensile). From eq 5, it can be seen that the size of the metallic domain increases linearly with temperature. A steep increase in the resonant frequency is observed at

dx.doi.org/10.1021/nl402116f | Nano Lett. 2013, 13, 4685−4689

temperatures beyond the transition temperature. Studies by Tsai et al.[35] and Schilbe et al.[36] indicate that the elastic modulus of VO_2 remains similar in both metallic and insulating phases. This increase in frequency can be interpreted as an increase in the strain of the nanowire.

The nanobeams used in our experiments are grown embedded in the substrate (at room temperature) and there can be a finite strain owing to growth conditions. Our observations suggest that this initial strain is tensile. After suspension (by etching the SiO_2 underneath with buffered HF solution), the state of tensile strain will be sustained due to clamping by the electrodes (refer to Supporting Information Section 1 for more details). At the onset of the insulating to metallic transition (M2−R transition), as seen from the phase diagram (Figure 2d), the strain is close to zero. The tension increases as the metallic R domain grows along the M2−R phase boundary (Figure 2d), since the R phase has a shrinkage in length along the longitudinal *c*-axis. Due to the constraint imposed by the contacts, the length of the resonator would remain the same, and the strain will keep on increasing resulting in a sharp rise in the resonant frequency. This is evident from the data of Figure 2a for temperatures greater than T_{c0}. The total strain, estimated from eq 5, is $[H/(E\varepsilon_0 T_{c0})](T - T_{c0})$. It is plotted in Figure 3. We rewrite eq 2 for resonant frequency as a function of temperature

$$f_0 = \sqrt{\frac{EI}{\rho S}}\left(\frac{1}{2L}\sqrt{\frac{H}{E\varepsilon_0 T_{c0}}\frac{S}{I}(T - T_{c0})} + \frac{1}{L^2}\right) \quad (7)$$

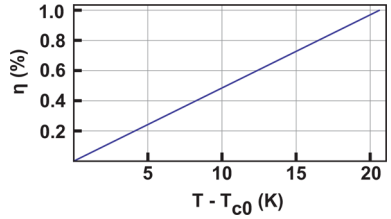

Figure 3. The calculated strain as a function of temperature when the metal domain develops. T_{c0} is the transition temperature of a free crystal of VO_2. If there is an initial tensile stress ε_i, the strain remains constant till $T = T_{c1}$ (see eq 5) and then starts increasing as per this plot.

This expression is plotted and visually compared with the experimental data of Figure 2a for high temperatures after the metal domain has appeared (Figure 4). The values of 140 GPa, 1020 Cal/mol, and 4500 kg/m^3 were used for elastic modulus, latent heat capacity, and mass density respectively.[35,36] The thickness *t* of the nanobeam is 266 nm as confirmed from the SEM images (refer to Supporting Information Section 1 for more details). In generating the plot, the suspension length (L), the moment of inertia I and free crystal transition temperature T_{c0} are taken as variable parameters. (The moment of inertia of a rectangular beam is $I_0 = (1/12)wt^3$. However, this estimate of I_0 assumes the ideal condition that the actuating electrostatic force is perpendicular to the "plane" face of the beam facing the gate electrode. This may not be the actual case for our devices, because of asymmetries in the orientation of the nanobeam with the gate electrode, resulting in a modified moment of inertia value. Also, the "effective" length of the resonator may be larger because the contacts may not act as perfectly rigid clamps.) The plot is shown in Figure 4. It is obtained for T_{c0} = 341.5 K, a suspension length (L) of 6.5 μm and a $I = 0.95I_0$. (The aforementioned value of suspension length is ∼18% larger than that obtained from the SEM image.) At higher temperatures, the calculated resonant frequency is larger than what we observe experimentally. The most probable cause of this difference is that the contacts do not serve as rigid clamps, which also makes the resonant frequencies lower than expected and an exact modeling of the system dynamics becomes difficult. Using the geometrical dimensions observed from the fit, we calculate the amount of temperature shift from the free crystal transition temperature (T_{c0}) at which the metal domain starts to grow. (This shift is given by $((\varepsilon_i\varepsilon_0 E T_{c0})/H)$ from eq 6.) It is estimated to be 2 K, which is in reasonable agreement with the occurrence of the "kink" in Figure 2a corresponding to the M2−R transition.

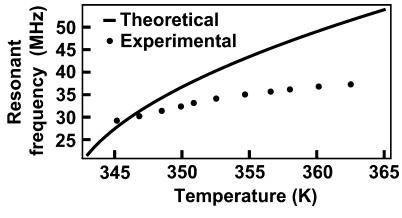

Figure 4. Calculated and experimental values of resonant frequency across the metal insulator transition. The solid line represents the calculated values and the experimental values are shown as discrete points.

In conclusion, simultaneous measurements of strain and resistance across metal−insulator transition in VO_2 nanobeam devices were carried out. The temperature dependent resistance measurements demonstrate an insulator−metal phase transition in the nanobeam. Changes in strain on the nanobeam across the metal−insulator transition are tracked by the resonance measurements indicating the development of tensile strain with the growth of the metallic domain. Signatures of the M1−M2 transition in the insulating phase are also seen. Our work shows that electromechanical resonance measurements can be effectively used to probe the phase transition phenomena when accompanied by lattice modifications. This method of studying elastic response can offer a much better precision than the traditional static stress−strain techniques. An improvement of the quality factor of devices and application of other nanomechanical measurement schemes (e.g., magnetomotive, optomechanical) provide a broad range of tools that may lead to new research directions in the field of phase transitions at nanoscale.

■ ASSOCIATED CONTENT

Ⓢ Supporting Information

Additional information and figures. This material is available free of charge via the Internet at http://pubs.acs.org.

■ AUTHOR INFORMATION

Corresponding Authors

*E-mail: shamashis@gmail.com.
*E-mail: deshmukh@tifr.res.in.

Author Contributions

‖P.P. and C.C. contributed equally to this work.

Notes

The authors declare no competing financial interest.

■ ACKNOWLEDGMENTS

The work at TIFR was supported by the Government of India. The work at Berkeley was supported by a NSF CAREER Award under Grant DMR-1055938.

■ REFERENCES

(1) Berglund, C. N.; Guggenheim, H. J. *Phys. Rev.* **1969**, *185*, 1022−1033.
(2) Morin, F. J. *Phys. Rev. Lett.* **1959**, *3*, 34−36.
(3) Goodenough, J. B. *Phys. Rev.* **1960**, *117*, 1442−1451.
(4) Zylbersztejn, A.; Mott, N. F. *Phys. Rev. B* **1975**, *11*, 4383−4395.
(5) Atkin, J. M.; Berweger, S.; Chavez, E. K.; Raschke, M. B.; Cao, J.; Fan, W.; Wu, J. *Phys. Rev. B* **2012**, *85*, 020101.
(6) Cao, J.; Gu, Y.; Fan, W.; Chen, L. Q.; Ogletree, D. F.; Chen, K.; Tamura, N.; Kunz, M.; Barrett, C.; Seidel, J.; Wu, J. *Nano Lett.* **2010**, *10*, 2667−2673.
(7) Wei, J.; Wang, Z.; Chen, W.; Cobden, D. H. *Nat. Nanotechnol.* **2009**, *4*, 420−424.
(8) Zhang, S.; Chou, J. Y.; Lauhon, L. J. *Nano Lett.* **2009**, *9*, 4527−4532.
(9) Fan, W.; Huang, S.; Cao, J.; Ertekin, E.; Barrett, C.; Khanal, D. R.; Grossman, J. C.; Wu, J. *Phys. Rev. B* **2009**, *80*, 241105.
(10) Jeong, J.; Aetukuri, N.; Graf, T.; Schladt, T. D.; Samant, M. G.; Parkin, S. S. P. *Science* **2013**, *339*, 1402−1405.
(11) Ji, H.; Wei, J.; Natelson, D. *Nano Lett.* **2012**, *12*, 2988−2992.
(12) Sengupta, S.; Wang, K.; Liu, K.; Bhat, A. K.; Dhara, S.; Wu, J.; Deshmukh, M. M. *Appl. Phys. Lett.* **2011**, *99*, 062114−062114−3.
(13) Sim, J. S.; Zhou, Y.; Ramanathan, S. *Nanoscale* **2012**, *4*, 7056−7062.
(14) Yang, Z.; Zhou, Y.; Ramanathan, S. *J. Appl. Phys.* **2012**, *111*, 014506−014506−5.
(15) Liu, K.; Fu, D.; Cao, J.; Suh, J.; Wang, K. X.; Cheng, C.; Ogletree, D. F.; Guo, H.; Sengupta, S.; Khan, A.; Yeung, C. W.; Salahuddin, S.; Deshmukh, M. M.; Wu, J. *Nano Lett.* **2012**, *12*, 6272−6277.
(16) Cao, J.; Ertekin, E.; Srinivasan, V.; Fan, W.; Huang, S.; Zheng, H.; Yim, J. W. L.; Khanal, D. R.; Ogletree, D. F.; Grossman, J. C.; Wu, J. *Nat. Nanotechnol.* **2009**, *4*, 732−737.
(17) Jones, A. C.; Berweger, S.; Wei, J.; Cobden, D.; Raschke, M. B. *Nano Lett.* **2010**, *10*, 1574−1581.
(18) Hu, B.; Ding, Y.; Chen, W.; Kulkarni, D.; Shen, Y.; Tsukruk, V. V.; Wang, Z. L. *Adv. Mater.* **2010**, *22*, 5134−5139.
(19) Abreu, E.; Liu, M.; Lu, J.; West, K. G.; Kittiwatanakul, S.; Yin, W.; Wolf, S. A.; Averitt, R. D. *New J. Phys.* **2012**, *14*, 083026.
(20) Qazilbash, M. M.; Brehm, M.; Chae, B. G.; Ho, P. C.; Andreev, G. O.; Kim, B. J.; Yun, S. J.; Balatsky, A. V.; Maple, M. B.; Keilmann, F.; Kim, H. T.; Basov, D. N. *Science* **2007**, *318*, 1750−1753.
(21) Wentzcovitch, R. M.; Schulz, W. W.; Allen, P. B. *Phys. Rev. Lett.* **1994**, *72*, 3389−3392.
(22) Eyert, V. *Ann. Phys.* **2002**, *11*, 650−702.
(23) Biermann, S.; Poteryaev, A.; Lichtenstein, A. I.; Georges, A. *Phys. Rev. Lett.* **2005**, *94*, 026404.
(24) Sohn, J. I.; Joo, H. J.; Ahn, D.; Lee, H. H.; Porter, A. E.; Kim, K.; Kang, D. J.; Welland, M. E. *Nano Lett.* **2009**, *9*, 3392−3397.
(25) Guo, H.; Chen, K.; Oh, Y.; Wang, K.; Dejoie, C.; Syed Asif, S. A.; Warren, O. L.; Shan, Z. W.; Wu, J.; Minor, A. M. *Nano Lett.* **2011**, *11*, 3207−3213.
(26) Guiton, B. S.; Gu, Q.; Prieto, A. L.; Gudiksen, M. S.; Park, H. *J. Am. Chem. Soc.* **2005**, *127*, 498−499.
(27) Yang, Y. T.; Callegari, C.; Feng, X. L.; Ekinci, K. L.; Roukes, M. L. *Nano Lett.* **2006**, *6*, 583−586.
(28) Chaste, J.; Eichler, A.; Moser, J.; Ceballos, G.; Rurali, R.; Bachtold, A. *Nat. Nanotechnol.* **2012**, *7*, 301−304.
(29) Hanay, M. S.; Kelber, S.; Naik, A. K.; Chi, D.; Hentz, S.; Bullard, E. C.; Colinet, E.; Duraffourg, L.; Roukes, M. L. *Nat. Nanotechnol.* **2012**, *7*, 602−608.
(30) Guerra, D. N.; Bulsara, A. R.; Ditto, W. L.; Sinha, S.; Murali, K.; Mohanty, P. *Nano Lett.* **2010**, *10*, 1168−1171.
(31) Rocheleau, T.; Ndukum, T.; Macklin, C.; Hertzberg, J. B.; Clerk, A. A.; Schwab, K. C. *Nature* **2010**, *463*, 72−75.
(32) Gouttenoire, V.; Barois, T.; Perisanu, S.; Leclercq, J. L.; Purcell, S. T.; Vincent, P.; Ayari, A. *Small* **2010**, *6*, 1060−1065.
(33) Sapmaz, S.; Blanter, Y. M.; Gurevich, L.; van der Zant, H. S. J. *Phys. Rev. B* **2003**, *67*, 235414.
(34) Wu, J.; Gu, Q.; Guiton, B. S.; de Leon, N. P.; Ouyang, L.; Park, H. *Nano Lett.* **2006**, *6*, 2313−2317.
(35) Tsai, K. Y.; Chin, T. S.; Shieh, H. P. D. *Jpn. J. Appl. Phys.* **2004**, *43*, 6268−6273.
(36) Schilbe, P.; Maurer, D. *Mater. Sci. Eng., A* **2004**, *370*, 449−452.
(37) Marezio, M.; McWhan, D. B.; Remeika, J. P.; Dernier, P. D. *Phys. Rev. B* **1972**, *5*, 2541−2551.
(38) Wall, S.; Wegkamp, D.; Foglia, L.; Appavoo, K.; Nag, J., Jr.; R. F., H.; Stähler, J.; Wolf, M. *Nat. Commun.* **2012**, *3*, 721.
(39) Kim, S.; Kim, K.; Kang, C. J.; Min, B. I. *Phys. Rev. B* **2013**, *87*, 195106.

Supporting Information: Dynamically tracking the strain across the metal-insulator transition in VO_2 measured using electromechanical resonators

Pritesh Parikh,[†,‡,§] Chitraleema Chakraborty,[†,§] T. S. Abhilash,[†] Shamashis Sengupta,[*,†] Chun Cheng,[¶] Junqiao Wu,[¶] and Mandar M. Deshmukh[*,†]

Department of Condensed Matter Physics and Materials Science, Tata Institute of Fundamental Research, Mumbai 400005, India , Birla Institute of Technology and Science - Pilani, Hyderabad 500078, India , and Department of Materials Science and Engineering, University of California, Berkeley, CA 94720, US

E-mail: shamashis@gmail.com; deshmukh@tifr.res.in

1. Device geometry

Scanning electron microscope image of a suspended VO_2 nanobeam device is shown in Fig. 1 (a). Here the devices are fabricated in four-probe geometry for resistance measurements and a local side gate is used for resonance measurements. Fig. 1 (b) shows the SEM image of the device in two probe geometry. As seen from the image, the length is measured to be 5.5 μm. Fig. 1 (c) shows the measurement for the thickness of the nanobeam. The pre-strain

[*]To whom correspondence should be addressed

[†]Department of Condensed Matter Physics and Materials Science, Tata Institute of Fundamental Research, Mumbai 400005, India

[‡]Birla Institute of Technology and Science - Pilani, Hyderabad 500078, India

[¶]Department of Materials Science and Engineering, University of California, Berkeley, CA 94720, US

[§]These authors contributed equally to this work.

due to growth conditions causes the nanobeams to buckle in certain cases, thereby affecting the nature of the insulator to metal transition. In the absence of buckling, the strain in the nanobeam manifests across the metal-insulator transition as a gradual decrease in the resistance concurrent with a sharp increase in resonant frequency due to the formation of metallic domains as seen in Fig. 2 (a),(c) of the main text (Fig. 1 (d)). The effect of contact resistance also causes the metal-insulator transition to be less pronounced (Fig. 2 (c) of the main text). Buckling introduces an addition level of complexity due to the non-uniformity in the strain across the nanobeam. Thus the transition is sharp without any metallic domains being formed as seen in Fig. 1 (b) of the main text (Fig. 1 (e)).

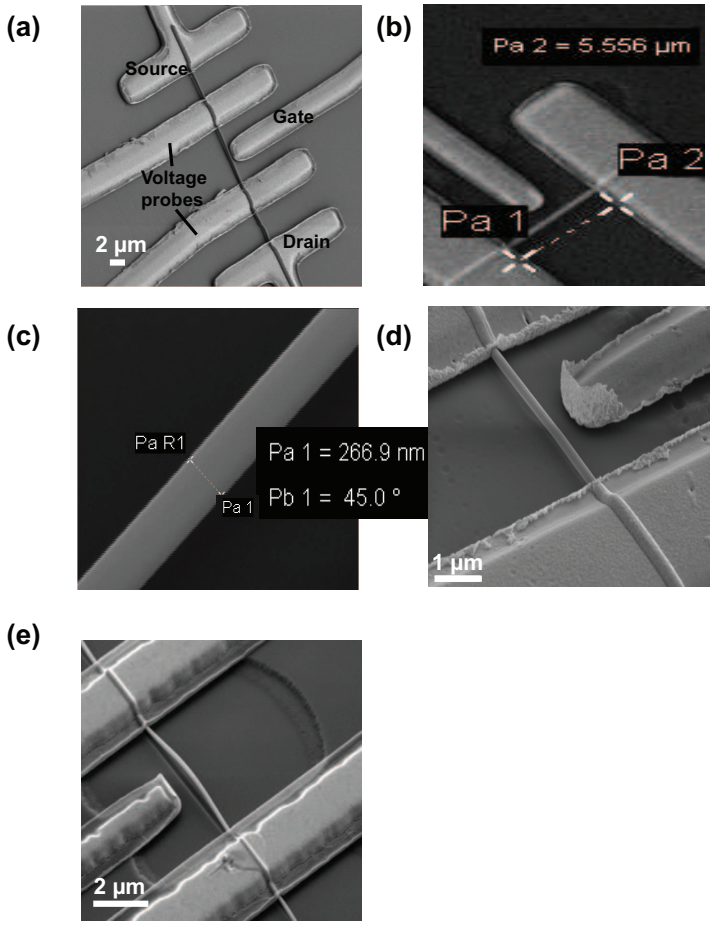

Figure 1: (a) Scanning electron microscope (SEM) image of the suspended nanobeam device in four probe geometry. SEM image of the suspended nanobeam device in two probe geometry (b) showing the measurement for the length and (c) thickness. SEM image with the VO_2 nanobeam (d) without buckling and (e) in the unstrained state (due to buckling).

2. Device Characteristics - Resistance and Resonance Plots

The resistance of the suspended nanobeam is measured as a function of temperature (Fig. 2 (a)). The measurements are carried out in an rf-probe station under vacuum conditions.

The resonant frequency shows a dispersion with the gate voltage. The observed frequency is given by an expression of the form

$$f = f_0 - \alpha(V_g^{dc})^2 + \beta(V_g^{dc})^4 \tag{1}$$

The $(V_g^{dc})^2$ term results from the spatial variation of the gate-induced electric field and the $(V_g^{dc})^4$ term reflects the influence of the gate-induced tension. The coefficients α and β depend upon various device parameters like geometry and elastic properties, and f_0 is the natural frequency of the resonator.[1]

Fig. 2(b) shows the variation of resonant frequency with gate voltage at room temperature (insulating phase) having negative dispersion, characteristics of softening of the effective spring constant.[1]

In Fig. 2 (c), we plot the resonance characteristics of a nanobeam device as a function of temperature. The corresponding resistance plot is shown in Fig. 2 (a). To measure the change in strain of the nanobeam across the metal-insulator transition, I_{mix} is measured as a function of the driving frequency f and the resonant frequency is tracked by varying the temperature (Fig. 2(c)). A dip in resonant frequency is observed at 309 K and 343 K. The dip in resonant frequency at 309 K corresponds to a M1-M2 phase transition. The large increase in frequency beyond 343 K can be interpreted as an increase in the strain of the nanobeam. A metal domain appears in this temperature range and the nanobeam shrinks along its length. As the size of the metal domain grows with increase in temperature, the intrinsic length of the nanobeam starts reducing and the strain is enhanced. This shows up as a sudden increase in the resonant frequency (Fig. 2(c)). Fig. 2 (d) shows the resonance peak in mixing current at temperatures 305 K (insulating phase) and 355 K (metallic phase).

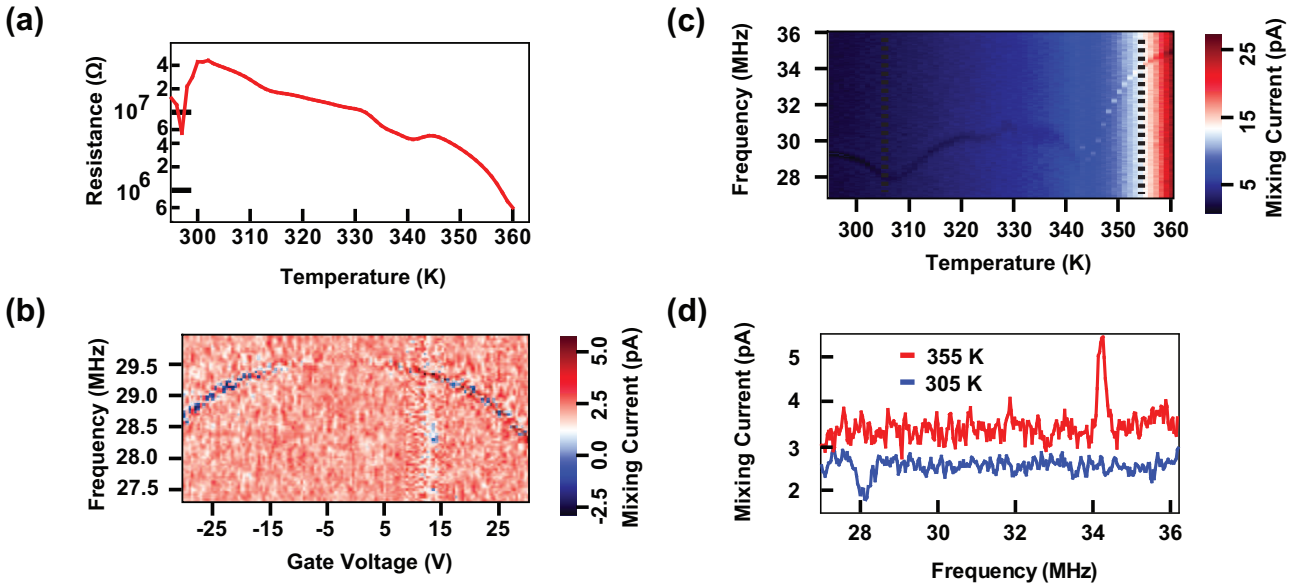

Figure 2: Device 2: (a) Resistance versus temperature plot. (b) Measured resonance response as a function of gate voltage (in the insulating phase at 295 K). (c) The resonant frequency of the device across the development of a metal domain from the purely insulating phase (d) Two line plots showing the resonant peak in mixing current data at temperatures before (305 K) and after (355 K) the sharp change in resonant frequency (the two line plots have been offset for clarity).

3. Resonance frequency Dispersion at different temperatures

The resonant frequency dispersion is plotted at different temperatures as the nanobeam is heated from 295 K to 360 K (across the insulator to metallic transition). The frequency dispersion disappears as the nanobeam becomes metallic. As seen from Fig. 3 the value of the resonant frequency at zero gate voltage changes with temperature, indicative of the fact that the strain state of the system is changing as the nanobeam undergoes an insulating to metallic transition.

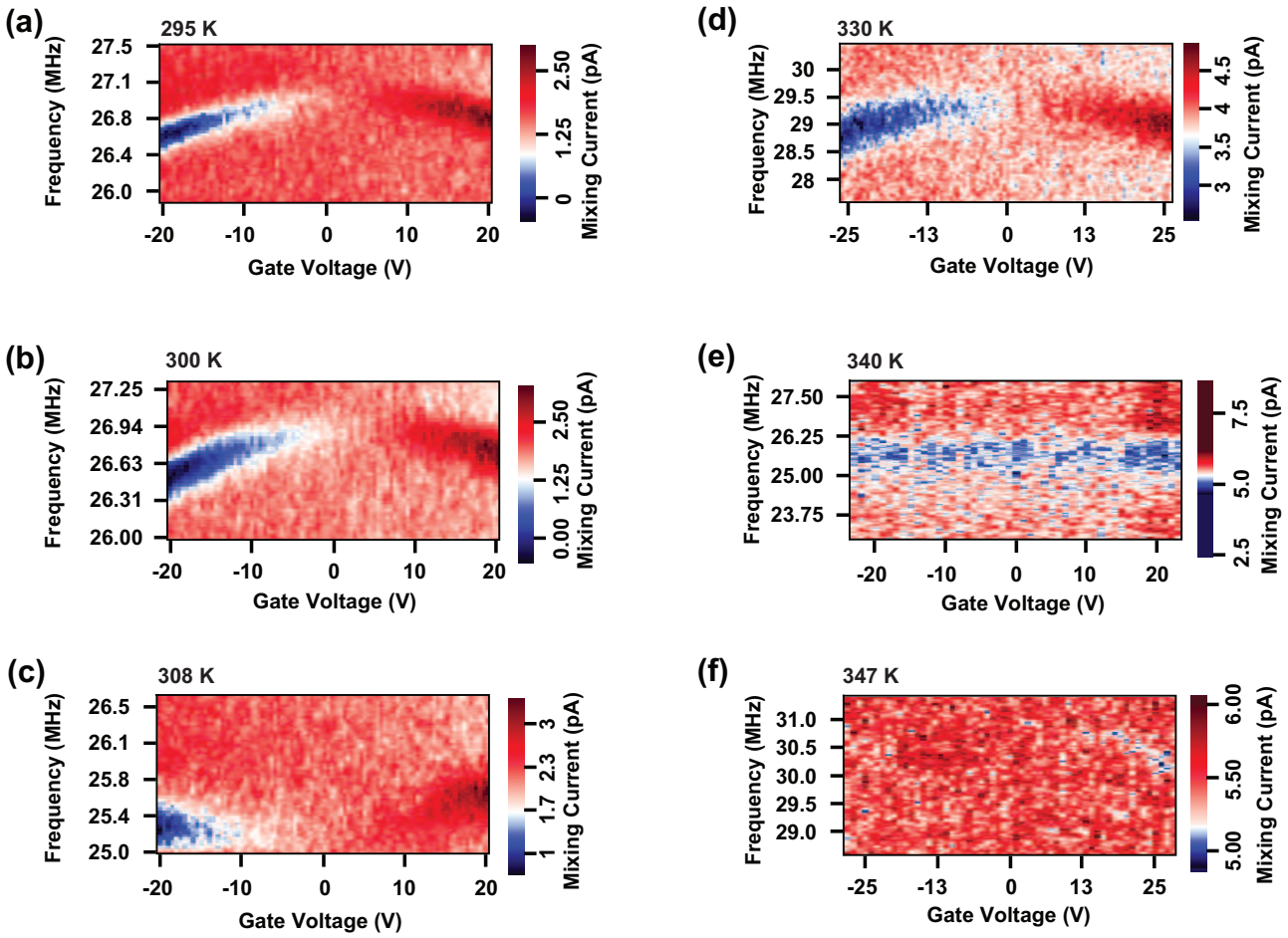

Figure 3: Shows resonant frequency dispersion with gate voltage at different temperatures (a) 295 K, (b) 300 K, (c) 308 K, (d) 330 K, (e) 340 K, (f) 347 K. Corresponding device resistance and resonance plots are shown in Fig. 2 of the main text.

4. Background subtraction

This section shows the unprocessed data and the background subtracted data. The unprocessed data is plotted in Fig. 4 right panel and the background subtracted data is shown in Fig. 2 of main text and Fig. 4 left panel.

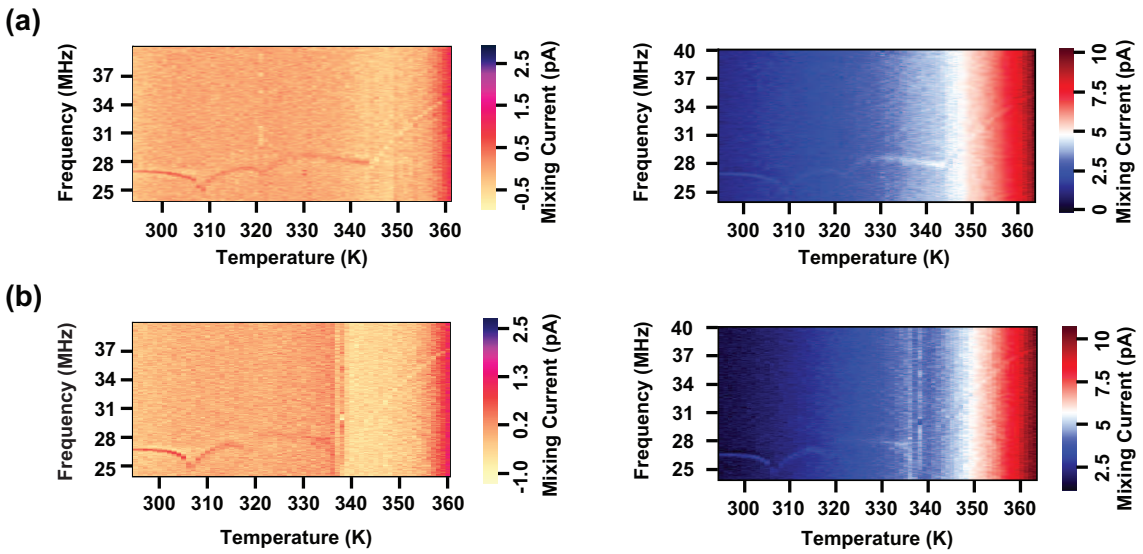

Figure 4: Left panel: Plots for background subtracted data, Right panel : Plots for the unprocessed data.

5. Additional Resistance Plots

This section shows plots for resistance measured as a function of temperature for two different set of devices.

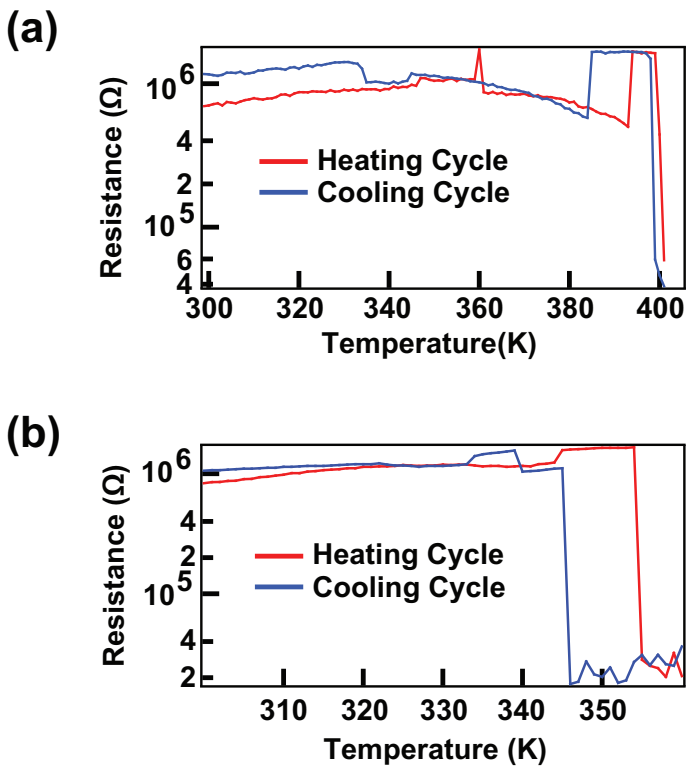

Figure 5: Resistance versus temperature plots for additional devices as shown in (a), (b).

References

(1) Solanki, H. S.; Sengupta, S.; Dhara, S.; Singh, V.; Patil, S.; Dhall, R.; Parpia, J.; Bhattacharya, A.; Deshmukh, M. M. *Physical Review B* **2010**, *81*, 115459.